Vibronic Structure of the Formyloxyl Radical (HCO_2) via Slow Photoelectron Velocity-Map Imaging Spectroscopy and Model Hamiltonian Calculations†

Etienne Garand,[‡] Kerstin Klein,[§,||] John F. Stanton,[*,§] Jia Zhou,[‡,⊥] Tara I. Yacovitch,[‡] and Daniel M. Neumark[*,‡,#]

Department of Chemistry, University of California, Berkeley, California 94720, Institute for Theoretical Chemistry and Department of Chemistry and Biochemistry, University of Texas at Austin, Austin, Texas 78712-0165, Johannes Gutenberg-Universität Mainz, Institut für Physikalische Chemie, D-55099 Mainz, Germany, and Chemical Sciences Division, Lawrence Berkeley National Laboratory, Berkeley, California 94720

Received: July 17, 2009; Revised Manuscript Received: August 11, 2009

We report high-resolution photoelectron spectra of HCO_2^- and DCO_2^- obtained with slow photoelectron velocity-map imaging. Well-resolved photodetachment transitions to the $^2A_1$ and $^2B_2$ states of the neutral radicals were observed. In addition, vibronic levels of the HCO_2 and DCO_2 radicals with up to 2000 cm^{-1} of internal energy were calculated using a quasidiabatic Hamiltonian approach and high-level ab initio calculations. Spectral simulations using the calculated levels were found to be in excellent agreement with the experimental spectra and used to assign many of its features. This study unambiguously determined that the $^2A_1$ state is the ground state of both HCO_2 and DCO_2, in contrast to earlier work that indicated the $^2B_2$ state was the ground state for DCO_2. For both isotopologs, the $^2B_2$ state is a very low-lying excited state with term energies of $T_0 = 318 \pm 8$ cm^{-1} for HCO_2 and $T_0 = 87 \pm 8$ cm^{-1} for DCO_2. The adiabatic electron affinities are determined to be EA(HCO_2) = 3.4961 ± 0.0010 eV and EA(DCO_2) = 3.5164 ± 0.0010 eV.

I. Introduction

The formyloxyl radical (HCO_2) is a reactive intermediate on the potential energy surface for the OH + CO reaction, a reaction of fundamental interest in combustion and atmospheric chemistry.[1−5] It is also a possible intermediate in the thermal decomposition of formic acid.[6,7] Formyloxyl also serves as a prototype for the more complex carboxyl free radicals such as CH_3CO_2, $PhCO_2$, and those derived from amino acids. This species has proven to be very difficult to characterize experimentally because of its metastability with respect to the H + CO_2 dissociation.[8−10] It also presents theoretical challenges owing to its two low-lying excited states, which strongly mix and result in a strong pseudo-Jahn−Teller (PJT) coupling that may or may not distort the ground-state equilibrium geometry from C_{2v} symmetry.[11−16] This coupling renders the accurate computation of the geometry and vibronic structure of this species difficult. In this paper, we characterize the vibronic structure of the HCO_2 and DCO_2 radicals using slow photoelectron velocity-map imaging (SEVI)[17] in combination with a theoretical treatment using a quasidiabatic Hamiltonian approach parametrized by high-level ab initio calculations.

The HCO_2 radical has proved rather elusive. The first reported observations of the formyloxyl radical were made on the basis of emission from vacuum ultraviolet photoexcited formic acid[18,19] and SCF molecular orbital calculations.[20] However, this emission could also have originated from formic acid itself.[21] While MacDonald and Sloan[22] found that the F + DCOOH reaction yielded HF and DF, suggesting that both HOCO and HCO_2 isomers were formed, a subsequent photoionization mass spectrometry study[8] of the same reaction found only HOCO and CO_2 products.

The first definitive observation of the HCO_2 and DCO_2 radicals was reported in 1995 by Kim et al.[9] using negative ion photoelectron (PE) spectroscopy of the formate anion, HCO_2^-. The C_{2v} geometry of HCO_2^- is well established,[23−27] so photodetachment of this anion provides a straightforward way to characterize the formyloxyl radical. Moreover, the three lowest neutral states ($^2A_1$, $^2B_2$ and $^2A_2$) can be accessed by one electron photodetachment from the ...$(1a_2)^2(4b_2)^2(6a_1)^2$ molecular orbital configuration of the HCO_2^- anion. Analysis of the PE spectra established the $^2A_1$ state as the ground state of HCO_2 with the $^2B_2$ state lying 0.027 ± 0.015 eV (218 ± 121 cm^{-1}) above. For DCO_2, the weak $^2B_2$ origin peak could not be resolved but it was estimated that the $^2B_2$ state was 0.008 eV (65 cm^{-1}) below the $^2A_1$ state.

Kim et al.[9] also carried out a vibrational analysis of the PE spectra with Franck−Condon simulations assuming C_{2v} symmetry for the anion and three neutral states. The vibrational modes in this symmetry are shown in Figure 1. There are three totally symmetric modes (ν_1−ν_3) with a_1 symmetry, one out-of-plane mode (υ_4) with b_1 symmetry, and two in-plane modes (ν_5, ν_6) with b_2 symmetry. Photodetachment transitions to all three states were dominated by progressions in the ν_3 mode, owing to the sensitivity of the OCO bend angle to the charge and electronic state of HCO_2, with considerably less activity in the ν_1 and ν_2 modes. The simulations performed reproduced many but not all features in the spectra, and the authors concluded that vibronic (PJT) coupling between the $^2A_1$ and $^2B_2$ states via the two vibrational modes of b_2 symmetry was responsible for additional peaks in the experimental spectrum. However, no quantitative assessment of vibronic coupling effects was performed.

† Part of the "W. Carl Lineberger Festschrift".

* Authors to whom correspondence should be addressed. E-mail address: dneumark@berkeley.edu (D.M.N.), jfstanton@mail.utexas.edu (J.F.S.).
‡ University of California.
§ University of Texas at Austin.
|| Johannes Gutenberg-Universität Mainz.
⊥ Current address: Chemical Dynamics Beamline, Lawrence Berkeley National Laboratory, Berkeley, California, 94720.
Lawrence Berkeley National Laboratory.

10.1021/jp9067894
Published on Web 09/08/2009

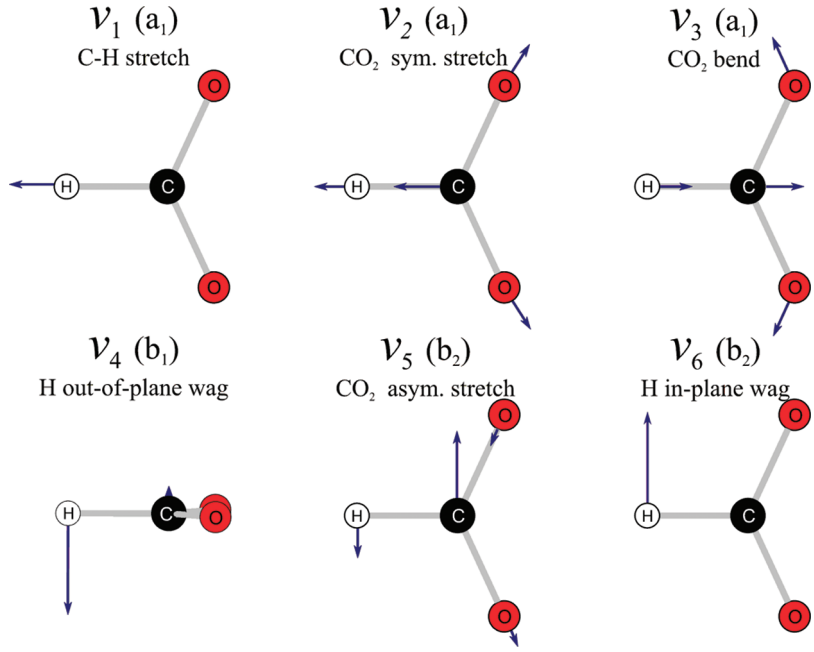

Figure 1. Normal coordinates displacement of the HCO_2 vibrational modes.

Clements and Continetti[10] also used the formate anion as a starting point to probe the formyloxyl radical dissociation dynamics via photoelectron-photofragment coincidence spectroscopy. They found that the three lowest neutral states of HCO_2 predissociate to H + CO_2.

The formyloxyl radical has also been the subject of several theoretical studies,[11−16,23] most of which were aimed at mitigating a tendency for this system to exhibit artifactual symmetry breaking effects and obtaining geometries for and energetics of the three lowest electronic states. However, even in quite sophisticated calculations, the splittings and energy ordering of these states cannot be determined with certainty. Some harmonic vibrational analyses also have been reported.[14−16] While these can be used to characterize the curvature of the various potential energy surfaces, they do not provide an accurate estimate of the vibronic level positions and zero-point energy corrections, owing to strong mixing between the different states.

In this paper, we report high-resolution SEVI spectra of HCO_2^- and DCO_2^- in the electron binding energy range of the $^2A_1$ and $^2B_2$ neutral states. The increased resolution afforded by SEVI allows the clear separation of the main peaks as well as the observation of several weaker transitions that were not discernible in the previous PE spectrum. Vibronic levels of the HCO_2 and DCO_2 radicals within 2000 cm^{-1} of the ground level are calculated using a quasidiabatic Hamiltonian approach parametrized by high-level ab initio calculations. Spectral simulations using the calculated levels are found to be in excellent agreement with the experimental spectra and are used to assign its dominant features. The combined experimental and theoretical analysis yields improved values for the electron affinities of HCO_2 and DCO_2, a revised assignment for the electronic ground state of DCO_2, and new insights into how vibronic coupling effects are manifested in photoelectron spectroscopy.

II. Experimental Section

The SEVI apparatus has been described in detail elsewhere.[17,28] SEVI is a high-resolution variant of PE spectroscopy in which mass-selected anions are photodetached at a series of wavelengths. The resulting photoelectrons are collected by velocity-map imaging (VMI)[29] using relatively low extraction voltages, with the goal of selectively detecting slow electrons with high efficiency and enlarging their image on the detector. At each wavelength, one obtains a high-resolution photoelectron spectrum over a limited range of electron kinetic energy.

In this experiment, HCO_2^- (DCO_2^-) anions were produced from a gas mixture comprising ~0.1% formic acid (formic acid-d_2) and 5% CO_2 in a balance of argon. The gas mixture, at a stagnation pressure of 300 psi, was expanded into the source vacuum chamber through an Even−Lavie pulsed valve[30] equipped with a grid discharge described in detail elsewhere.[31] Anions formed in the gas expansion were perpendicularly extracted into a Wiley−McLaren time-of-flight mass spectrometer[32] and directed to the detachment region by a series of electrostatic lenses and pinholes. Anions were photodetached between the repeller and the extraction plates of the VMI stack by the gently focused frequency-doubled output of a Nd:YAG pumped tunable dye laser. The photoelectron cloud formed was then coaxially extracted down a 50 cm flight tube and mapped onto a detector comprising a chevron-mounted pair of time-gated, imaging quality microchannel plates coupled to a phosphor screen, as is typically used in photofragment imaging experiments.[33] Events on the screen were collected by a 1024 × 1024 charge-coupled device (CCD) camera and sent to a computer. Electron velocity-mapped images resulting from 50 000 to 100 000 laser pulses were summed, quadrant symmetrized, and inverse-Abel transformed.[34] Photoelectron spectra were obtained via angular integration of the transformed images. The spectra presented here are plotted with respect to electron binding energy (eBE), defined as the difference between the energy of the photodetachment photon and the measured electron kinetic energy (eKE).

The apparatus was calibrated by acquiring SEVI images of atomic chloride at several different photon energies. With the −350 V VMI repeller voltage used in this study, the Gaussian width (2σ) of the chloride peaks were 4.2 cm^{-1} at 31 cm^{-1} eKE and 28 cm^{-1} at 916 cm^{-1}. Line widths in the spectra presented here (~15 cm^{-1}) are limited by unresolved rotational structure; since the origin of

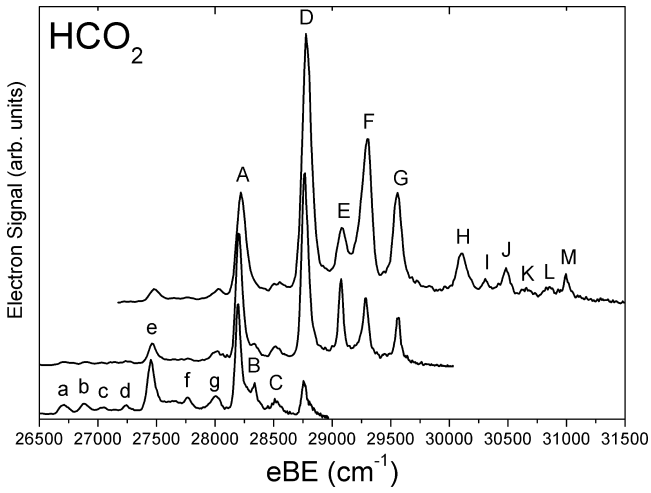

Figure 2. SEVI spectra of HCO_2^- between the electron binding energies of 26 500 and 31 500 cm^{-1}. The three traces were taken at photon energies of 31 745, 30 030, and 28 986 cm^{-1} and are vertically offset for clarity.

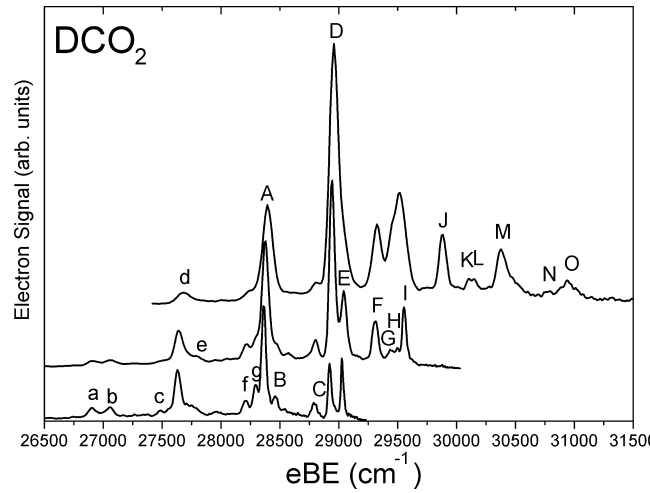

Figure 3. SEVI spectra of DCO_2^- between the electron binding energies of 26 500 and 31 500 cm^{-1}. The three traces were taken at photon energies of 32 023, 30 052, and 29 240 cm^{-1} and are vertically offset for clarity.

an unresolved rotational profile may not be aligned with the observed peak maximum, we report error bars of one Gaussian standard deviation (σ) for all energy determinations.

SEVI also provides information on the photoelectron angular distribution (PAD). For one-photon detachment, the PAD is given by[35,36]

$$\frac{d\sigma}{d\Omega} = \frac{\sigma_{total}}{4\pi}\left(1 + \beta\left(\frac{3}{2}\cos^2(\theta) - \frac{1}{2}\right)\right) \quad (1)$$

where θ is the angle between the direction of the photoelectron ejection and the polarization vector of the incident photon. The anisotropy parameter β is sensitive to the shape and symmetry of the anion molecular (technically, Dyson) orbital from which detachment occurs. It lies between +2 and −1, yielding limiting PADs of the form $\cos^2\theta$ and $\sin^2\theta$, respectively.

III. Results

SEVI spectra of HCO_2^- and DCO_2^- in the electron binding energy range 26 500− 31 500 cm^{-1} are shown in Figures 2 and 3, respectively. This spectral range includes the features that were assigned to the $^2A_1$ and $^2B_2$ neutral states in the previous PE spectra,[9] although the PE spectra covered a considerably larger range of eBE. Each figure shows three traces corresponding to different photodetachment energies that are vertically offset for clarity. The peak positions, shifts from the origin, and PADs are summarized in Table 1. The value of β depends on the detachment energy[37] and thus peaks having $0 < \beta < 0.3$ are simply labeled as "s" while those with $\beta > 1$ are labeled as "p".

The SEVI spectra presented here are similar to the previous PE spectra.[9] However, the increased resolution afforded by SEVI allows clear separation of the main peaks as well as several weaker transitions that were not discernible in the previous study. In Figures 2 and 3, the peaks labeled A, which have "p" PAD's and are found at 28 198 and 28 362 cm^{-1} for HCO_2^- and DCO_2^-, respectively, correspond to the features that were previously assigned as the origin transitions to the $^2A_1$ state. For HCO_2, the origin transition to the low-lying $^2B_2$ state was assigned to a feature corresponding to the small peak labeled C, with "s" PAD, at 28 516 cm^{-1}, and this assignment is confirmed in the work presented here. The SEVI spectra of HCO_2 reveals another weak peak labeled B with the same "s" PAD and located below peak C, at 28 239 cm^{-1}; this feature is assigned as a sequence band (see section V). The DCO_2 spectra show a similar pattern with peaks B and C at 28 449 and 28 792 cm^{-1}, respectively. However, our analysis indicates that for this isotopolog, peak B is the origin transition for photodetachment to the $^2B_2$ state. Several weak peaks are also found below peak A in both spectra and are labeled with the lowercase letters a−g.

Comparison of the traces in Figures 2 and 3 shows that the relative intensities of some features in the SEVI spectra change as the photon energy is varied. This effect reflects the Wigner threshold law,[37,38] which defines the photodetachment cross

TABLE 1: HCO_2^- SEVI Spectral Peak Positions, Shifts from Origin and PAD as Well as the Calculated Frequencies and Assignments

peak	eBE (cm^{-1})	shift from origin (cm^{-1})	PAD[a]	calculated position (cm^{-1})	assignment[b]
a	26 713	−1485	p	−1504	$3_2^0(^2A_1)$
b	26 889	−1309	p	−1325	$2_1^0(^2A_1)$
c	27 042	−1156	s	−1194	$3_2^0(^2B_2)$
d	27 240	−958	p	−934	$3_2^1(^2A_1)$
e	27 455	−743	p	−752	$3_1^0(^2A_1)$
f	27 763	−435	s	−442	$3_1^0(^2B_2)$
g	28 002	−196	p	−182	$3_1^1(^2A_1)$
A	28 198	0	p	0.0	$0_0^0(^2A_1)$
B	28 329	131	s	128	$3_1^1(^2B_2)$
C	28 516	318	s	310.2	$0_0^0(^2B_2)$
D	28 762	564	p	569.7	$3_0^1(^2A_1)$
				569.9	6_0^1 ($^2A_1$)
E	29 075	877	s	880.1	$3_0^1(^2B_2)$
F	29 284	1086	p	1058.8	$3_0^2(^2A_1)$
				1075.4	$3_0^1 6_0^1(^2A_1)$
				1145.4	$2_0^1(^2A_1)$
G	29 561	1363	s	1337.1	$6_0^2(^2A_1) + 6_0^1(^2B_2)$
				1387.6	$3_0^2 6_0^1(^2A_1) + 3_0^2(^2B_2)$
H	30 108	1910	p	1872.1	$3_0^1 6_0^2(^2A_1)$
				1939.8	highly mixed
				1968.6	highly mixed
I	30 307	2109	p		
J	30 482	2284	s		
K	30 650	2452	p		
L	30 855	2657	p		
M	30 999	2801	*s*		

[a] Peaks with $0 < \beta < 0.3$ are labeled as "s" while those with $\beta > 1$ are labeled as "p". [b] The transitions are labeled according to their best harmonic oscillator and diabatic electronic state representation, whenever possible.

TABLE 2: DCO_2^- SEVI Spectral Peak Positions, Shifts from Origin and PAD as Well as the Calculated Frequencies and Assignments

peak	eBE (cm^{-1})	shift from origin (cm^{-1})	PAD[a]	calculated position (cm^{-1})	assignment[b]
a	26 903	−1459	p	−1489	$3_2^0(^2A_1)$
b	27 057	−1305	p	−1312	$2_1^0(^2A_1)$
c	27 486	−876		−811	$3_2^1(^2B_2)$
d	27 630	−732	p	−745	$3_1^0(^2A_1)$
e	27 720	−642		−645	$3_1^0(^2B_2)$
f	28 207	−155	p	−180	$3_1^1(^2A_1)$
g	28 294	−68	s	−67	$3_1^1(^2B_2)$
A	28 362	0	p	0.0	$0_0^0(^2A_1)$
B	28 449	87	s	100.5	$0_0^0(^2B_2)$
C	28 792	430	s	399.8	$6_0^1(^2A_1)$
D	28 925	563	p	564.8	$3_0^1(^2A_1)$
E	29 028	666	s	677.8	$3_0^1(^2B_2)$
F	29 310	948	s	910.0	$3_0^16_0^1(^2A_1)$
				970.2	$6_0^1(^2B_2)$
G	29 446	1084	p	1068.3	$3_0^2(^2A_1)$
H	29 498	1136	p	1138.6	$2_0^1(^2A_1)$
I	29 555	1193	s	1199.7	$3_0^2(^2B_2)$
J	29 882	1520	p	1478.1	$1_0^1(^2A_1)$
				1492.6	$3_0^16_0^2$ $(^2A_1)$
K	30 105	1743	s	1770.0	highly mixed
L	30 153	1791	s	1835.9	highly mixed
M	30 385	2023	p	1997.4	highly mixed
N	30 780	2418			
O	30 945	2583	p		

[a] Peaks with $0 < \beta < 0.3$ are labeled as "s" while those with $\beta > 1$ are labeled as "p". [b] The transitions are labeled according to their best harmonic oscillator and diabatic electronic state representation, whenever possible.

section (σ) as a function of the energy above threshold (ΔE) and the orbital angular momentum of the ejected electron (l):

$$\sigma \propto (\Delta E)^{l+1/2} \tag{2}$$

Thus, as the photon energy is lowered, the intensity of peaks with "s" PAD's increases with respect to those with "p" PAD's, as seen previously.[39,40]

IV. Theoretical Framework

i. Model Hamiltonian. Calculations of the vibronic level structure of HCO_2 and DCO_2 were made using the quasidiabatic Hamiltonian approach of Köppel, Domcke, and Cederbaum (KDC).[41] The parametrization of the Hamiltonian used in this work is, however, considerably more elaborate than in typical applications of the KDC method. While a full discussion of the theoretical approach taken in the HCO_2 and DCO_2 calculations will be deferred to a subsequent detailed theoretical paper,[42] it is appropriate to give an outline here.

For the present calculations, which are designed to be accurate for states within roughly 0.25 eV (2000 cm^{-1}) of the ground vibronic level, only the $^2A_1$ and $^2B_2$ electronic states of the radical were considered. The $^2A_2$ state, clearly seen in the earlier experiments by Kim et al.[9] at ca. 0.5 eV, was excluded. More extended calculations of the spectrum, which are ongoing, demonstrate that the effects of coupling to the $^2A_2$ state are negligible in the energy range pertinent to this study. Thus, the quasidiabatic Hamiltonian has the general form

$$H = \begin{pmatrix} T_{AA} & 0 \\ 0 & T_{BB} \end{pmatrix} + \begin{pmatrix} V_{AA} & V_{AB} \\ V_{AB} & V_{BB} \end{pmatrix} \tag{3}$$

where the kinetic energy is assumed diagonal and A and B stand for the $^2A_1$ and $^2B_2$ electronic states, respectively. The theoretical foundation for this form of the Hamiltonian is extensively discussed Köppel et al.[41] and more recently by Ichino et al.,[43] where the interested reader is referred for details. The construction of **V** in this work follows the spirit of the "adiabatic parameterization" approach described by Ichino et al.,[44] and each block of the potential matrix is expressed as a polynomial in the basis of the dimensionless normal coordinates of the anion, viz.

$$V^A = E_0 + \sum_i F_i^A q_i + \frac{1}{2}\sum_{ij} F_{ij}^A q_i q_j + \ldots \tag{4}$$

$$V^B = E_0 + \Delta_0 + \sum_i F_i^B q_i + \frac{1}{2}\sum_{ij} F_{ij}^B q_i q_j + \ldots \tag{5}$$

$$V^{AB} = \sum_i \lambda_i q_i + \ldots \tag{6}$$

where E_0 is arbitrary and Δ_0 is the energy spacing between the two neutral states at the origin of the coordinate system (chosen as the anion geometry).

For HCO_2 and DCO_2, the Taylor expansion of the diagonal blocks of the potential contains terms up to quartic in the totally symmetric modes (ν_1, ν_2, and ν_3), and through quadratic for the coupling modes (ν_5 and ν_6). All anharmonic mixing between the symmetric and coupling modes is assumed to be zero in the quasidiabatic basis. The out-of-plane distortion, ν_4, has b_1 symmetry and does not couple the two states considered here; it is therefore active only through even-quantum transitions from the ground state which, in any event, do not appear to be seen in the range of the spectrum that is relevant to this paper. Its effect is seen only implicitly in terms of the energy gap between the two electronic states, as discussed at the end of this subsection.

As elaborated elsewhere,[44] the quasidiabatic and adiabatic (quantum chemical) potentials are coincident along the totally symmetric coordinates. Consequently, the corresponding potential constants (those that carry indices 1, 2, and 3 only) were obtained from straightforward ab initio calculations (see next subsection). In accord with the adiabatic parametrization approach, constants for the $^2B_2$ and $^2A_1$ states were evaluated at the corresponding minimum energy geometries. The coupling constants, which appear only in the off-diagonal block of the potential, were calculated analytically in the framework of the quasidiabatic ansatz and formalism of Ichino et al.[43]

The coupling constants in this particular molecular system show a pronounced geometrical dependence, particularly those for v_6 with regard to the symmetric CO_2 symmetric stretch and bend modes (ν_2 and ν_3). Values of the coupling constants λ_5 and λ_6 at the $^2A_1$ equilibrium geometry for HCO_2 are 2109 and 1341 cm^{-1}, respectively; at the geometry of the $^2B_2$ state, the corresponding values are 2127 and 491 cm^{-1}. The coordinate dependence of λ_6 is so large that efforts to simulate the spectrum with an intermediate constant value were unsuccessful. Thus, the coupling constants were parametrized as follows. At the equilibrium geometries of the $^2A_1$ and $^2B_2$ states, the coupling constants λ_5 and λ_6 were evaluated analytically. It was then assumed that the constants vary linearly with displacement along the symmetric modes, i.e.

$$\lambda_i = \lambda_i^0 + \sum_{k=1}^{3} \lambda_{ik} q_k \quad (7)$$

The bilinear terms were first calculated by finite difference of analytic coupling constants around the reference geometry (that of the anion, which is between the two final state equilibrium geometries). The values ultimately used in the parametrization were obtained by scaling these "vertical" derivatives such that the coupling constants coincide with the analytic values at the final state equilibrium geometries. That is, the first-order variation of the coupling constants is constrained to the proportionality conditions that exist at the reference geometry but scaled such that the final state coupling constants match the ab initio calculations at the final state geometries. Quasidiabatic quadratic force constants (F_{ij}) that govern the coupling modes (ν_5 and ν_6) were then determined from the corresponding adiabatic force constant (f_{ij}) and coupling parameters via the easily derived and well-known second-order perturbation theory relation:[43]

$$F_{ij} = f_{ij} + \frac{2\lambda_i\lambda_j}{E - E'} \quad (8)$$

where E is the energy of the state of interest at its equilibrium geometry and E' is the energy of the state to which it is coupled via λ_i and λ_j.

The final step in the adiabatic parametrization procedure is to express the potential constants discussed above, in which the expansion points are the minima of the final states, in terms of an expansion about the common reference geometry. This is a straightforward transformation in which force constants of a given order are determined by displacements of the final states relative to the reference state (D_i) and all of the same and higher order force constants (those expressed with respect to the final state geometries).[42] This technically applies to all of the constants, but the diabatic force constants for the coupling modes are, by construction, independent of the origin of the coordinate system since they are not present in the anharmonic part of the *quasidiabatic* potential. All anharmonicity involving ν_5 and ν_6 in the *adiabatic* potentials is carried by the coupling constants. The resulting potential matrix, when diagonalized, gives adiabatic surfaces that satisfy the following criteria:

(1) The adiabatic potentials, through quartic terms in the symmetric coordinates and quadratic terms in the nonsymmetric (coupling) coordinates, coincide precisely with those given by the ab initio calculations *at the minima of the final states.*

(2) The displacements from the reference (anion) geometry to the final state equilibrium geometries are the same as those given by the ab initio calculation, while the vertical energy gap is unaffected by the coordinate transformation.

Other features of the ab initio adiabatic potentials are not precisely reproduced, namely the vertical distance between the states at the final state equilibrium geometries, the gradient of the final state surfaces at the origin of the coordinate system (the vertical geometry), the adiabatic force fields of the states at the vertical (and other nonequilibrium) geometries, etc. The extent to which the latter parameters deviate from the ab initio values is related to how faithfully the Taylor expansions of the quasidiabatic potential blocks represent the physics of the problem in the relevant range of displacements. While a detailed discussion of this issue will appear in the forthcoming paper,[42] suffice it to say that with the quartic expansion used here, the representation of the actual adiabatic surfaces is excellent over the entire region of the potential surface that are relevant to the present spectroscopic study.

TABLE 3: Parameters Appearing in the Off-Diagonal Block of the Model Hamiltonian[a]

parameter	HCO_2	DCO_2
λ_5^0	2115	2017
λ_{15}	−13	−24
λ_{25}	1	11
λ_{35}	2	11
λ_6^0	894	896
λ_{16}	16	15
λ_{26}	−163	−144
λ_{36}	−93	−83

[a] See text for the definitions. All quantities in cm^{-1}.

All parameters used in the calculations are given in Table 3 and 4. The vertical gap Δ_0 (eq 5) of 1337 cm^{-1} obtained in the ab initio calculations was shifted by +40 cm^{-1} to approximately reproduce the splitting of the two origin bands in the HCO_2 spectrum, and further adjusted to account for the zero-point energy in the neglected ν_4 mode. The calculated harmonic frequencies for ν_4 are 1017 and 834 cm^{-1} for HCO_2 in the $^2B_2$ and $^2A_1$ states, respectively. Thus, the differential zero point energy (in the harmonic approximation) between the two states is 92 cm^{-1} which, when added to the shifted ab initio vertical energy difference of 1377 cm^{-1}, gives the value of Δ_0 found in the leftmost column (top row) of Table 4. For DCO_2, the corresponding ab initio harmonic frequencies are 847 and 754 cm^{-1}, for a zero-point differential Δ_0 of 46 cm^{-1}. Thus, the parametrization of the Hamiltonian is "honest", apart from the shift of the vertical gap, and essentially purely ab initio. No empirical scaling or other fudge factors are used; the only assumption made is that of linear behavior for the coupling constants. The calculations were performed in a direct product harmonic oscillator vibronic basis using 30 functions for the totally symmetric modes, and 15 basis functions for the coupling modes ν_5 and ν_6. The total size of the basis was 12 150 000 functions, and 3000 Lanczos recursions were performed to ensure convergence of the vibronic level positions to ca. 2 cm^{-1}. The calculations required only a few hours on a laptop computer and are not computationally demanding. Assignments of the calculated level positions to a diabatic electronic state and vibrational mode were made on the basis of visual inspection of the nodal properties of the corresponding eigenvector. At relatively low energies, this was usually straightforward, but at higher energies the substantial mixing of zeroth-order states was so great, that some assignments were not attempted.

ii. Quantum Chemical Calculations. The adiabatic potentials were obtained with the coupled-cluster singles and doubles method,[45] as augmented with a perturbative treatment of triple excitations (CCSD(T)).[46] Minima and quadratic force constants were determined and calculated with the aid of analytic first[47−49] and second[50] derivative techniques, and the quartic potential surfaces found in Table 4 were determined from numerical fits of a 9 × 9 × 9 grid (721 points) of energies evaluated at specific displacements in terms of the normal coordinates of the anion. These calculations used the atomic natural orbital (ANO) basis set of Taylor and Almlöf,[51] truncated to 4s3p2d1f on C and O, and 4s2p1d on H. Core electrons were not included in the correlation treatment, and the spherical harmonic representations of the d and f polarization functions were used.

Quasidiabatic coupling constants were calculated analytically[43] with the equation-of-motion coupled-cluster technique

TABLE 4: Quasidiabatic Force Constants (F) at the $^2B_2$ and $^2A_1$ Minimum Energy Geometries in the Reduced Normal Coordinate Representation of the Anion[a]

	HCO_2		DCO_2			HCO_2		DCO_2	
	$^2B_2$	$^2A_1$	$^2B_2$	$^2A_1$		$^2B_2$	$^2A_1$	$^2B_2$	$^2A_1$
Δ_0	1469	0	1423	0	F_{122}	−21	−92	42	−47
D_1	0.075	−0.245	0.302	−0.420	F_{133}	−11	28	−15	32
D_2	−1.594	0.437	−1.548	0.339	F_{233}	20	−63	17	−57
D_3	−1.998	3.524	−2.034	3.527	F_{123}	−31	−20	−28	−29
F_{11}	3651	2048	2745	1423	F_{1111}	1528	1062	836	582
F_{22}	1631	959	1556	1009	F_{2222}	45	−3	47	3
F_{33}	565	755	562	742	F_{3333}	15	−8	15	−8
F_{12}	−292	250	−215	238	F_{1112}	−113	−80	17	10
F_{13}	−53	55	−37	85	F_{1113}	−35	−23	1	−1
F_{23}	158	−330	154	−318	F_{2223}	−31	−28	−25	−28
F_{55}	1533	1915	1481	1964	F_{1122}	0	3	−7	−4
F_{66}	1234	920	941	628	F_{1133}	0	5	−2	6
F_{56}	239	−308	186	−186	F_{2233}	−19	19	−18	16
F_{111}	−2519	−1894	−1609	−1234	F_{1222}	5	8	−3	8
F_{222}	−338	−107	−330	−134	F_{1333}	−2	−4	42	−47
F_{333}	57	9	56	9	F_{2333}	−6	10	−15	32
F_{112}	192	211	−24	51	F_{1123}	0	3	17	−57
F_{113}	67	48	16	7	F_{1223}	9	−1	−28	−29
F_{223}	47	140	36	133	F_{1233}	2	−9	836	582

[a] Also included are the displacements (D_i) between the final state minima and the equilibrium structure of the anion, and the vertical energy gap Δ_0, as adjusted for the differential zero-point energy of the out-of-plane ν_4 mode (see text for details).

known as EOMIP-CCSD[52] using the double-ζ plus polarization (DZP) basis sets.[53] As the implementation is new, it was necessary to correlate all electrons in these calculations, due to an unresolved issue in how to treat orbital relaxation effects in such calculations when core orbitals are omitted. The variation of coupling constants with geometry was calculated by evaluating the constants analytically at fixed displacements of the nuclei along the three totally symmetric coordinates; derivatives were then obtained by central difference. This is a legitimate procedure in terms of the quasidiabatic ansatz of ref 43, and is, to our knowledge, the first time that bilinear coupling constants have been calculated in a direct fashion. All ab initio calculations used the CFOUR program system.

iii. Adiabatic Potential Energy Surfaces. Diagonalization of the quasidiabatic potential (second term in eq 3) yields the adiabatic potential energy surfaces associated with the two lowest electronic states of formyloxyl. Along the totally symmetric coordinates these are, as mentioned above, identical to the diagonal blocks of **V** (the off-diagonal matrix element vanishes if the nuclear framework has C_{2v} symmetry) and are not particularly interesting. For HCO_2 and other molecules that exhibit strong pseudo-Jahn−Teller (PJT) effects, the dependence of the adiabatic potential along the coupling modes can be a very sensitive function of the diabatic coupling strength[54] (corresponding to λ_5 and λ_6 for HCO_2). If the coupling exceeds a threshold for a given energy gap Δ between the two states ($|\lambda_i| > [F_{ii}\Delta/2]^{1/2}$), the adiabatic potential with respect to the coordinate q_i becomes a double minimum with a local maximum at the high symmetry point. Thus, small energy gaps and/or large coupling strengths can act to distort the adiabatic potential surfaces so profoundly that the point group of the equilibrium geometry has a symmetry lower than that of the high-symmetry structure that must always prevail in the absence of coupling.[55]

For HCO_2, a pictorial representation of the lowest adiabatic surface is given in Figure 4. Due to the fact that there are five relevant coordinates, the coordinate axes in Figure 4 do not correspond to simple isolated normal coordinate displacements. Each point of the potential represented in the figure corresponds to the energy of the lowest adiabatic state at a particular value of the *anion* coordinates q_3 and q_6 (which roughly correspond to the CO_2 bend (a_1) and the H in-plane wag (b_2), with the energy optimized with respect to all other coordinates. The salient feature of the potential, which will be discussed in more detail in ref 42, is that the minimum energy C_{2v} geometry associated with the $^2A_1$ electronic state is *not* a minimum on the adiabatic potential energy surface. That is, from the perspective of a quantum chemist, this electronic state of HCO_2 is "not C_{2v}" at the level of theory employed here. However, the magnitude of the barrier (which is less than 20 cm^{-1}) is so small as to be well below the zero-point level; this little "dimple" in the potential thus has no particular physical relevance. As is amply demonstrated by this work, photodetachment of the anion to the $^2A_1$ state of formyloxyl can be quite satisfactorily described within a C_{2v} framework; the observation of non-Franck−Condon transitions to levels involving odd number of quanta in the ν_5 and ν_6 coupling modes can be understood only in terms of vibronic coupling, in which the potential energy surface picture of the Born−Oppenheimer approximation is not strictly applicable, anyway.

In contrast to the $^2A_1$ state, the $^2B_2$ electronic state of formyloxyl is much simpler, exhibiting a pronounced minimum at the C_{2v} geometry. In terms of the quasidiabatic model Hamiltonian, the striking difference between the adiabatic potential for $^2A_1$ and $^2B_2$ states is a direct consequence of the coordinate dependence of λ_6 (see Table 3); at large values of the OCO angle, the coupling is significantly stronger than at small values of θ_{OCO}. It should be noted that the other possibility—that the vertical gap between the two electronic states is significantly smaller at the $^2A_1$ geometry—is not operative in this example. At the CCSD(T)/ANO1 level, the vertical energy differences between the states is 10 866 cm^{-1} at the $^2B_2$ geometry and 10 945 cm^{-1} at the $^2A_1$ geometry, a surprisingly small difference that is insignificant in the context of this discussion. Thus, the adiabatic potential of the state with the larger bond angle (144.8° for the $^2A_1$ state at the CCSD(T)/ANO1 level of theory vs 112.5° for $^2B_2$) is more profoundly influenced by the coupling. Another experimental finding that can be rationalized in terms of the adiabatic potentials is the significantly smaller value of ν_6 in the $^2A_1$ state of DCO_2, 430 cm^{-1}, compared to 860 cm^{-1} for the $^2B_2$ state. Finally, it should

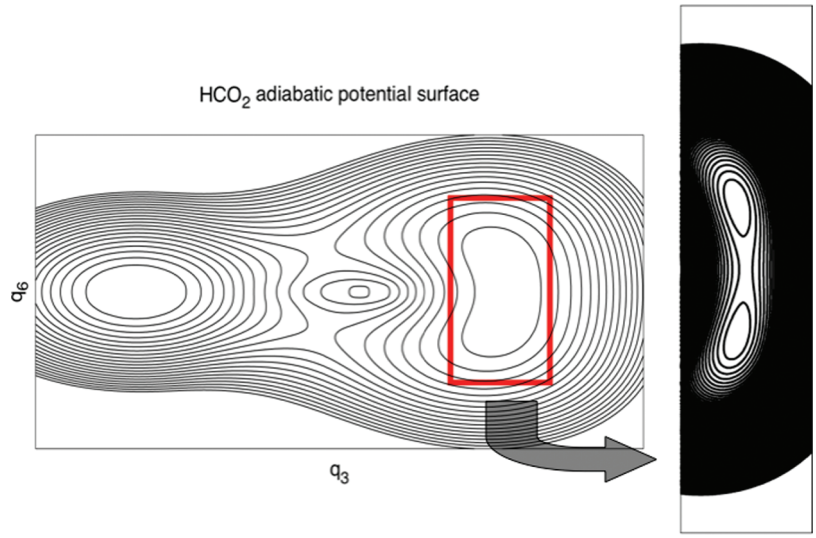

Figure 4. Contour representation of the lower adiabatic sheet of the potential energy surface for the formyloxyl radical, obtained by diagonalizing the model potential described in section IVi. At each point (q_3, q_6), the adiabatic energy is that obtained when all other coordinates are varied so as to minimize the energy. The $^2B_2$ region of the potential is that at lower values of q_3 (to the left of the conical intersection). The contour level is 100 cm^{-1}, and the region in the immediate vicinity of the $^2A_1$ minimum energy geometry is expanded in the inset to show the nearly negligible double minimum. Points along the line $q_6 = 0$ have C_{2v} symmetry; all other geometries have C_s symmetry with unequal CO bond distances and HCO bond angles. Note that both "electronic states" lay on the same adiabatic sheet of the potential surface and may interconvert by pseudorotation.

be pointed out that the rather large difference in state splitting between the normal and deuterated isotopologues is due in part to the fact that CH(D) bond is substantially different in the two diabatic states, with a calculated harmonic frequency of 3106 and 2333 cm^{-1}, respectively for ν_1 in the A_1 and B_2 states of HCO_2. More about the nature of the adiabatic potentials of these two states, as well as the somewhat higher-lying $^2A_2$ state, will be discussed in ref 42.

V. Discussion

Simulated spectra of HCO_2^- and DCO_2^- are shown as the lower plots in Figures 5 and 6, respectively. The present simulations are limited to transitions to neutral states within 2000 cm^{-1} of the ground level. The stick spectra show the calculated positions and intensities of the individual transitions. Transitions to levels with A_1 and B_2 vibronic symmetries are shown in red and blue, respectively. The gray shaded spectra represent the sum of the A_1 and B_2 transitions convoluted with a 20 cm^{-1} full width at half-maximum Gaussian function. The top trace in each figure is a composite experimental spectrum made by joining parts of the three SEVI traces shown in Figures 2 and 3. The composite spectrum is constructed from sections of the three SEVI traces that were not close to either the maximum and minimum electron binding energy. Each section was individually scaled to match the intensity of the SEVI spectrum taken at the highest photon energy and then spliced together at points that fall on the baseline. For the simulated HCO_2 and DCO_2 spectra, the calculated origin transition was aligned with the experimental peak labeled "A". The simulated spectra agree well with experiment, allowing straightforward assignment of the dominant features in the HCO_2^- and DCO_2^- SEVI spectra. These assignments are summarized in Table 1 and 2 along with the calculated positions of the corresponding vibronic levels. In these tables as well as in the following discussion, the transitions are labeled according to their best harmonic oscillator and diabatic electronic state representation, whenever possible.

Peak A in the HCO_2 spectrum is the vibrational origin transition of the $^2A_1$ state. The weak peak labeled C, lying 318 cm^{-1} above peak A, is assigned to the vibrational origin of the $^2B_2$ state. This assignment implies that features having "p" and "s" PADs correspond to transitions to neutral levels having A_1 and B_2 vibronic symmetry, respectively. Peaks D, F, and H in the HCO_2 spectrum, have "p" PADs and are thus assigned to A_1 levels. Specifically, peaks D and F are assigned to the 3_0^1 and $3_0^2(^2A_1)$ transitions, respectively, while peak H is assigned to the $3_0^1 6_0^2(^2A_1)$ transition as well as a transition to a highly mixed level of A_1 vibronic symmetry. A transition to another highly mixed state of B_2 symmetry with a calculated position of 1968.6 cm^{-1} might also contribute to peak H.

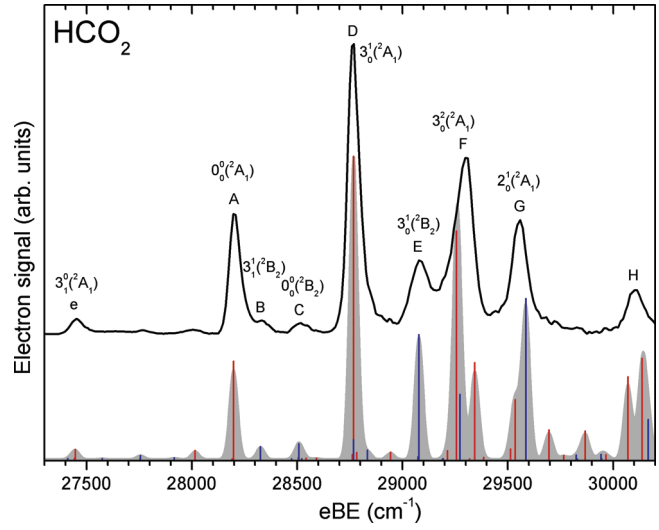

Figure 5. Comparison between the HCO_2^- SEVI spectrum and the simulated spectrum. The calculated transitions to levels having A_1 and B_2 vibronic symmetries are shown in red and blue, respectively. The gray shaded spectra represent the sum of the A_1 and B_2 transitions convoluted with a 20 cm^{-1} Gaussian width. The top trace is a composite experimental spectra made by joining parts of the 3 traces shown in Figure 2.

Peak B, E, and G have "s" PADs and are thus assigned to transitions to B_2 levels. Peak E, which lies 877 cm^{-1} above the $^2A_1$ origin, is assigned to the $3_0^1(^2B_2)$ transition while peak G is

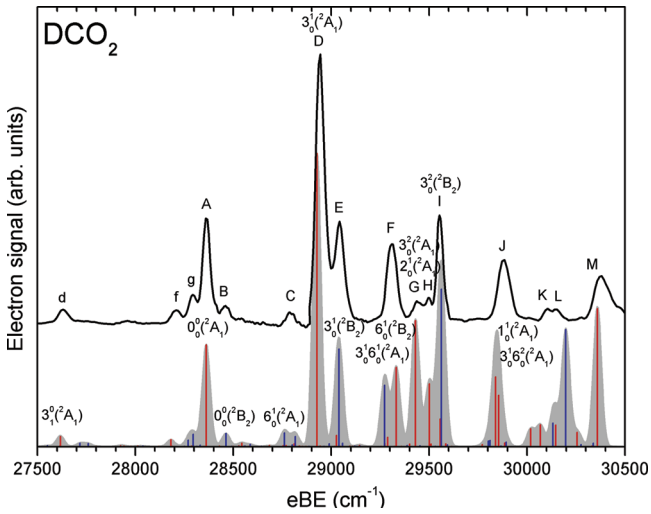

Figure 6. Comparison between the DCO_2^- SEVI spectrum and the simulated spectrum. The calculated transitions to levels having A_1 and B_2 vibronic symmetries are shown in red and blue, respectively. The gray shaded spectra represent the sum of the A_1 and B_2 transitions convoluted with a 20 cm^{-1} Gaussian width. The top trace is a composite experimental spectra made by joining parts of the three traces shown in Figure 3.

assigned to a transition to a quite mixed level of B_2 symmetry, best described as $6_0^1(^2A_1) + 3_0^2(^2B_2)$, with a possible contribution from another transition to a mixed level of A_1 symmetry that is best described as $6_0^2(^2A_1) + 6_0^1(^2B_2)$. The small peak B, which lies 131 cm^{-1} above peak A, is apparently not a transition from the anion ground vibrational state. Its assignment is discussed later with the other hot bands.

Similarly, the simulations and the PADs can be used to assign most features in the DCO_2 spectrum. Peaks A, D, G, H, J, and M all have "p" PAD's and are assigned to transitions to A_1 symmetry levels. Peak A is the vibrational origin transition to the $^2A_1$ state. Peaks D and G, which lie 563 and 1084 cm^{-1} above the $^2A_1$ origin, are assigned to the $3_0^1(^2A_1)$ and $3_0^2(^2A_1)$ transitions, respectively, while peak H is assigned to the $2_0^1(^2A_1)$ transition. Peak J is assigned to the overlapped $1_0^1(^2A_1)$ and $3_0^1 6_0^2(^2A_1)$ transitions, while peak M at 2023 cm^{-1} is assigned to a transition to a highly mixed level with A_1 symmetry.

Peaks B, C, E, F, I, K, and L all have "s" PADs and are thus assigned to transitions to levels with B_2 vibronic symmetry. The weak peak labeled B, lying only 87 cm^{-1} above the origin is assigned as the vibrational origin transition to the $^2B_2$ electronic state. This assignment is in good agreement with the calculated $^2B_2 - ^2A_1$ splitting of 100.5 cm^{-1} in DCO_2. This assignment differs from the previous PE spectrum where the weak transition to the $^2B_2$ ground level could not be resolved. In that spectrum, the $^2B_2$ state was tentatively assigned as the DCO_2 ground state lying ~65 cm^{-1} below the $^2A_1$ state. Peaks E and I are assigned to the $3_0^1(^2B_2)$ and $3_0^2(^2B_2)$ transitions, respectively. The weak peak C is assigned to the $6_0^1(^2A_1)$ transition, while peak F is assigned to the overlapped $3_0^1 6_0^1$ ($^2A_1$) and $6_0^1(^2B_2)$ transitions; all three transitions are allowed only by vibronic coupling. Finally, the weak peaks K and L are assigned to highly mixed levels with B_2 vibronic symmetry.

Compared to the HCO_2^- SEVI spectrum, the DCO_2^- spectrum shows more peaks that are unambiguously allowed by vibronic coupling, most notably peaks C and F. This result does not imply stronger vibronic coupling between the DCO_2 states; it reflects the observation that the ν_3 and ν_6 frequencies are nearly the same for the $^2A_1$ state of HCO_2, whereas they differ for the $^2A_1$ state of DCO_2. Hence, in the simulated HCO_2^- spectrum, the weak, vibronically allowed $6_0^1(^2A_1)$ transition occurs at the same energy as the much stronger, fully allowed $3_0^1(^2A_1)$ transition (peak D, Figure 5), so a distinct $6_0^1(^2A_1)$ transition is not observed.

Peaks I−J in the HCO_2^- spectrum as well as peaks N and O in the DCO_2^- spectrum lie more than 2000 cm^{-1} above the origin transition and are thus not included in the present calculations. From the trend observed in both the HCO_2^- and DCO_2^- spectra, these are probably transitions to highly mixed $^2A_1$ and $^2B_2$ levels that cannot readily be described by the usual harmonic oscillator and diabatic electronic state notation. The second excited state ($^2A_2$), which lies ~0.5 eV above the $^2A_1$ ground state, might also contribute to these peaks. More accurate calculations involving all three low-lying states are ongoing.[42]

Several very weak peaks, labeled a−g, are also found in the HCO_2^- and DCO_2^- spectra at lower eBE than the origin transitions. These features are assigned to transitions originating from excited vibrational levels of the respective anions and are well-reproduced by the simulations, assuming an anion vibrational temperature of ~400 K. Peaks e and a are assigned to the $3_1^0(^2A_1)$ and $3_2^0(^2A_1)$ transitions, respectively. This assignment yields a value of 743 cm^{-1} for the υ_3 fundamental in HCO_2^- which is in excellent agreement with the 744.1 cm^{-1} value measured in the Ne matrix.[24] Using this value and the 563 cm^{-1} υ_3 fundamental for the neutral HCO_2 ($^2A_1$) determined previously, we can assign peaks d and g to the $3_2^1(^2A_1)$ and $3_1^1(^2A_1)$ transitions, respectively. Similarly, peaks f and c are assigned to the $3_1^0(^2B_2)$ and $3_2^0(^2B_2)$ transitions, respectively. Peak B, lying 131 cm^{-1} above the origin transition, can be assigned to the $3_1^1(^2B_2)$ transition. The remaining small peak b is assigned to the $2_1^0(^2A_1)$ transition, yielding a 1309 cm^{-1} υ_2 fundamental for HCO_2^-. This value agrees with the frequency of 1323 cm^{-1} measured in a Ne matrix[24] and the ab initio value of 1325 cm^{-1} obtained at the CCSD(T)/ANO1 level using second-order vibrational perturbation theory.[42] The same process can be applied to the weak peaks labeled a−g in the DCO_2^- spectrum to assign them to similar hot band transitions involving the υ_2 and υ_3 modes. This analysis yields values of 1305 and 732 cm^{-1} for the DCO_2^- υ_2 and υ_3 fundamentals, respectively. These are again in excellent agreement with the 1309.1 and 736.9 cm^{-1} frequencies obtained from Ne matrix isolation experiments[24] and the corresponding ab initio fundamentals at 1311 and 745 cm^{-1}.[42]

The present study unambiguously determines that the $^2A_1$ electronic state is the ground state of both HCO_2 and DCO_2, in contrast to the previous assignment for DCO_2.[9] The adiabatic electron affinities are given by the position of the peak labeled "A" in both spectra and are determined to be $EA(HCO_2) = 3.4961 \pm 0.0010$ eV and $EA(DCO_2) = 3.5164 \pm 0.0010$ eV. The $^2B_2$ electronic state is found to be a very low-lying excited state with term energies of $T_0(^2B_2) = 0.0394 \pm 0.0010$ eV (318 $\pm$ 8 cm^{-1}) for HCO_2 and $T_0(^2B_2) = 0.0108 \pm 0.0010$ eV (87 $\pm$ 8 cm^{-1}) for DCO_2. Electron affinities, term values, and vibrational fundamentals determined in this work are summarized in Table 5.

The calculated term energies for the $^2B_2$ state are within a few wavenumbers of the experimental values, which is a very good indication of the accuracy of the ab initio method and quasidiabatic Hamiltonian approach used in this study. Moreover, most of the calculated vibronic level positions are found to be within 40 cm^{-1} of the experimental values. There are, however, some notable discrepancies between the simulated spectrum and the experiment with regard to the relative intensity

TABLE 5: Experimental Spectroscopic Constants Determined in This Work[a]

	EA (eV)	$T_0(^2B_2)$ (eV)	anion (X^1A_1)		neutral ($^2A_1$)			neutral ($^2B_2$)
			ν_2	ν_3	ν_2	ν_3	ν_6	ν_3
HCO_2	3.4961	0.0394	1309	743		564		559
DCO_2	3.5164	0.0108	1305	732	1136	563	430	579

[a] All the vibrational frequencies are in cm^{-1}. The error bar on all numbers is ± 8 cm^{-1} (± 0.0010 eV).

of some of the features. Most of these can be explained in term of the Wigner threshold law, which modulates the relative intensity of the "s" and "p" features as a function of detachment photon energy and is not taken into account in the simulations.

The present work demonstrates how the combination of SEVI and state-of-the-art theory provides a powerful tool to unravel the complex vibronic structure of open-shell species. With respect to conventional PE spectroscopy, the high resolution afforded by SEVI allows the clear observation of close-lying and weak bands which otherwise would be strongly overlapping. A good example of this is the weak $^2B_2$ origin peak in the DCO_2 spectrum which could not be resolved from the stronger $^2A_1$ origin in the previous PE study and led to an erroneous assignment of the DCO_2 ground state. Moreover, in contrast to anion zero electron kinetic energy (ZEKE) spectroscopy,[56] a photodetachment technique with comparable resolution, SEVI retains the ability of photoelectron spectroscopy to observe transitions involving photoelectrons ejected with nonzero orbital angular momentum. In the present case, all the transitions to levels with B_2 vibronic symmetry (blue sticks in Figures 3 and 4), which proceed mainly by p-wave detachment, would not have been observed with ZEKE, thus limiting the amount of spectroscopic information that could be obtained from the spectra.

On the other hand, the results presented here showcase the need for detailed theory to interpret SEVI spectra, especially when the neutral species is subject to strong pseudo-Jahn−Teller coupling. For example, the nominally forbidden $6_0^1(^2A_1)$ and $3_0^1 6_0^1(^2A_1)$ transitions are observed in the DCO_2 spectrum. These transitions have the same "p" PADs as the $^2B_2$ electronic state from which they "borrow" intensity through vibronic coupling, similar to what was observed in CCS[39] and C_2H.[40] In the case of DCO_2, such an assignment is difficult to make a priori, because the $^2A_1$ and $^2B_2$ bands overlap one another. Under these circumstances, neither the intensites nor positions of the vibronically allowed transitions can be predicted with simple models. The theoretical treatment presented here thus provides an essential complement to the SEVI spectra by allowing the unambiguous assignment of the observed features.

VI. Conclusions

We report high-resolution SEVI photodetachment spectra of HCO_2^- and DCO_2^- to probe the $^2A_1$ and $^2B_2$ electronic states of the corresponding radicals. Vibronic levels of the HCO_2 and DCO_2 radicals with up to 2000 cm^{-1} of internal energy are calculated with a quasidiabatic Hamiltonian parametrized by high-level ab initio calculations. Spectral simulations using the calculated levels are found to be in good agreement with the experimental spectra and are used to assign most of its features. The combination of the spectral resolution of SEVI and the high-level calculations reported here shows that the $^2A_1$ state is the ground state of both HCO_2 and DCO_2 species. The $^2B_2$ state is found to be a very low-lying excited state with term energies of $T_0 = 318 \pm 8$ cm^{-1} for HCO_2 and $T_0 = 87 \pm 8$ cm^{-1} for DCO_2. Several gas-phase vibrational frequencies of the formyloxyl radical and formate anion were also determined for the first time.

Acknowledgment. This work was supported by the Air Force Office of Scientific Research under Grant No. F49620-03-1-0085 (D.M.N), and the U.S. Department of Energy, Basic Energy Sciences [Contract FG02-07ER15884] and the Robert A. Welch Foundation (J.F.S). K.K. was supported for a semester in Austin through funding from the Deutsche Forschungsgemeinschaft (DFG GA 370/5-1). E.G. thanks the National Science and Engineering Research Council of Canada (NSERC) for a post graduate scholarship and T.Y. thanks the Fonds Québécois de la Recherche sur la Nature et les Technologies (FQRNT) for a master's scholarship. J.F.S. and K.K. also thank Takatoshi Ichino (Austin) for discussions concerning the adiabatic parametrization procedure used in this work.

References and Notes

(1) Schatz, G. C.; Fitzcharles, M. S.; Harding, L. B. *Faraday Discuss.* **1987**, *84*, 359.
(2) Bradley, K. S.; Schatz, G. C. *J. Chem. Phys.* **1997**, *106*, 8464.
(3) Duncan, T. V.; Miller, C. E. *J. Chem. Phys.* **2000**, *113*, 5138.
(4) Yu, H. G.; Muckerman, J. T.; Sears, T. J. *Chem. Phys. Lett.* **2001**, *349*, 547.
(5) Song, X. L.; Li, J. C.; Hou, H.; Wang, B. S. *J. Chem. Phys.* **2006**, 125.
(6) Francisco, J. S. *J. Chem. Phys.* **1992**, *96*, 1167.
(7) Goddard, J. D.; Yamaguchi, Y.; Schaefer, H. F. *J. Chem. Phys.* **1992**, *96*, 1158.
(8) Ruscic, B.; Schwarz, M.; Berkowitz, J. *J. Chem. Phys.* **1989**, *91*, 6780.
(9) Kim, E. H.; Bradforth, S. E.; Arnold, D. W.; Metz, R. B.; Neumark, D. M. *J. Chem. Phys.* **1995**, *103*, 7801.
(10) Clements, T. G.; Continetti, R. E. *J. Chem. Phys.* **2001**, *115*, 5345.
(11) Peyerimhoff, S. D.; Skell, P. S.; May, D. D.; Buenker, R. J. *J. Am. Chem. Soc.* **1982**, *104*, 4515.
(12) Feller, D.; Huyser, E. S.; Borden, W. T.; Davidson, E. R. *J. Am. Chem. Soc.* **1983**, *105*, 1459.
(13) McLean, A. D.; Lengsfield, B. H.; Pacansky, J.; Ellinger, Y. *J. Chem. Phys.* **1985**, *83*, 3567.
(14) Rauk, A.; Yu, D.; Borowski, P.; Roos, B. *Chem. Phys.* **1995**, *197*, 73.
(15) Stanton, J. F.; Kadagathur, N. S. *J. Mol. Struct.* **1996**, *376*, 469.
(16) Ayala, P. Y.; Schlegel, H. B. *J. Chem. Phys.* **1998**, *108*, 7560.
(17) Neumark, D. M. *J. Phys. Chem. A* **2008**, *112*, 13287.
(18) Style, D. W. G.; Ward, J. C. *Trans. Faraday Soc.* **1953**, *49*, 999.
(19) Suto, M.; Wang, X. Y.; Lee, L. C. *J. Phys. Chem.* **1988**, *92*, 3764.
(20) Peacock, T. E.; Rias-ur-Rahman; Sleeman, D. H.; Tuckley, E. S. G. *Discuss. Faraday Soc.* **1963**, 144.
(21) Lee, Y. P.; Pimentel, G. C. *J. Chem. Phys.* **1981**, *74*, 4851.
(22) Macdonald, R. G.; Sloan, J. *J. Chem. Phys.* **1978**, *31*, 165.
(23) Dixon, D. A.; Feller, D.; Francisco, J. S. *J. Phys. Chem. A* **2003**, *107*, 186.
(24) Forney, D.; Jacox, M. E.; Thompson, W. E. *J. Chem. Phys.* **2003**, *119*, 10814.
(25) Kidd, K. G.; Mantsch, H. H. *J. Mol. Spectrosc.* **1981**, *85*, 375.
(26) Krekeler, C.; Mladenovic, M.; Botschwina, P. *Phys. Chem. Chem. Phys.* **2005**, *7*, 882.
(27) Zachariasen, W. H. *J. Am. Chem. Soc.* **1940**, *62*, 1011.
(28) Osterwalder, A.; Nee, M. J.; Zhou, J.; Neumark, D. M. *J. Chem. Phys.* **2004**, *121*, 6317.
(29) Eppink, A.; Parker, D. H. *Rev. Sci. Instrum.* **1997**, *68*, 3477.
(30) Even, U.; Jortner, J.; Noy, D.; Lavie, N.; Cossart-Magos, C. *J. Chem. Phys.* **2000**, *112*, 8068.
(31) Garand, E.; Yacovitch, T. I.; Neumark, D. M. *J. Chem. Phys.* **2009**, *130, 064304.*
(32) Wiley, W. C.; McLaren, I. H. Rev. Sci. Instrum. **1955**, *26*, 1150.
(33) Chandler, D. W.; Houston, P. L. *J. Chem. Phys.* **1987**, *87*, 1445.
(34) Hansen, E. W.; Law, P. L. *Opt. Soc. Am. A* **1985**, *2*, 510.
(35) Cooper, J.; Zare, R. N. *J. Chem. Phys.* **1968**, *48*, 942.
(36) Reid, K. L. *Annu. Rev. Phys. Chem.* **2003**, *54*, 397.
(37) Wigner, E. P. *Phys. Rev.* **1948**, *73*, 1002.
(38) Reed, K. J.; Zimmerman, A. H.; Andersen, H. C.; Brauman, J. I. *J. Chem. Phys.* **1976**, *64*, 1368.
(39) Garand, E.; Yacovitch, T. I.; Neumark, D. M. *J. Chem. Phys.* **2008**, *129, 074312.*

(40) Zhou, J.; Garand, E.; Neumark, D. M. J. Chem. Phys. **2007**, *127*, 114313.
(41) Koppel, H.; Domcke, W.; Cederbaum, L. S. *Adv. Chem. Phys.* **1984**, *57*, 59.
(42) Klein, K.; Gauss, J.; Garand, E.; Neumark, D. M.; Stanton, J. F. Manuscript in preparation.
(43) Ichino, T.; Gauss, J.; Stanton, J. F. *J. Chem. Phys.* **2009**, *130*, 174105.
(44) Ichino, T.; Gianola, A. J.; Lineberger, W. C.; Stanton, J. F. *J. Chem. Phys.* **2006**, *125, 084312.*
(45) Purvis, G. D.; Bartlett, R. J. J. Chem. Phys. **1982**, *76*, 1910.
(46) Raghavachari, K.; Trucks, G. W.; Pople, J. A.; Headgordon, M. *Chem. Phys. Lett.* **1989**, *157*, 479.
(47) Lee, T. J.; Rendell, A. P. *J. Chem. Phys.* **1991**, *94*, 6229.
(48) Scuseria, G. E. *J. Chem. Phys.* **1991**, *94*, 442.
(49) Watts, J. D.; Gauss, J.; Bartlett, R. J. *Chem. Phys. Lett.* **1992**, *200*, 1.
(50) Gauss, J.; Stanton, J. F. *Chem. Phys. Lett.* **1997**, *276*, 70.
(51) Almlöf, J.; Taylor, P. R. *J. Chem. Phys.* **1987**, *86*, 4070.
(52) Stanton, J. F.; Gauss, J. *J. Chem. Phys.* **1995**, *103*, 8931.
(53) Redmon, L. T.; Purvis, G. D.; Bartlett, R. J. *J. Am. Chem. Soc.* **1979**, *101*, 2856.
(54) Stanton, J. F. *J. Chem. Phys.* **2007**, *126*, 134309.
(55) Bersuker, I. B.; Balabanov, N. B.; Pekker, D.; Boggs, J. E. *J. Chem. Phys.* **2002**, *117*, 10478.
(56) Kitsopoulos, T. N.; Waller, I. M.; Loeser, J. G.; Neumark, D. M. *Chem. Phys. Lett.* **1989**, *159*, 300.

JP9067894